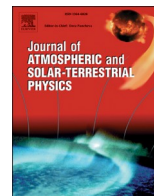




Contents lists available at ScienceDirect

Journal of Atmospheric and Solar–Terrestrial Physics

journal homepage: www.elsevier.com/locate/jastp

Research Paper

A method to derive global O/N₂ ratios from SSUSI/DMSP based on Re-AURIC algorithmGuangXing Ding^a, Bo Chen^{a,*}, XiaoXin Zhang^b, Fei He^c^a Changchun Institute of Optics, Fine Mechanics and Physics, Chinese Academy of Sciences, Changchun, 130033, China^b National Center for Space Weather/National Satellite Meteorological Center, China Meteorological Administration, Beijing, 100000, China^c Key Laboratory of Earth and Planetary Physics, Institute of Geology and Geophysics, Chinese Academy of Sciences, Beijing, 100000, China

ARTICLE INFO

Keywords:

O/N₂ ratio
Re-AURIC
FUV dayglow
Magnetic storm

ABSTRACT

Global thermospheric O/N₂ column density ratios are obtained using the SSUSI/DMSP far-ultraviolet (FUV) dayglow data and the Re-AURIC simulation results. The Re-AURIC is derived from the AURIC algorithm after some old modules are updated. The calculation processes of O/N₂ ratio are then established using the simulations of Re-AURIC to calibrate the ratios of the OI 135.6 nm emission and N₂ LBHS emission from SSUSI observations. The standard deviation (1σ) and correlation coefficient are 0.045 and 0.769 compared with the O/N₂ ratios provided by the SSUSI EDR data. The statistical errors between the calculated ratios and the EDR references are generally less than 0.2 with 96.40% at 2σ (95.44%) and less than 0.1 with 60.51% at about 1σ (68.26%). Two global O/N₂ ratio maps are obtained using this method to study its variations when the magnetic storm occurs. The significant O/N₂ depletion can be seen in one O/N₂ ratio map whose Kp index is 6. Also, the depletion is not uniform at different longitudes and the scales extend from high latitude to low latitude during magnetic storm. This proposed method provides us with a simple and useful tool to obtain the global O/N₂ distribution and even the future modeling from the observations on satellites.

1. Introduction

During the past several years, the need to monitor, assess, and even forecast space weather in the thermosphere and beyond has become a strong focus within the community. Measurements of the ratios of atomic oxygen and molecular nitrogen emissions are particularly sensitive to compositional changes (Meier and Anderson, 1983; Strickland et al., 1995; Evans et al., 1995), which in turn reflect dynamical responses to external forcing. When solar storms break, the solar wind carrying a large number of particles attack the atmosphere, Joule heating and energetic particles' deposition, result in an increase in temperature and a decrease in O/N₂ in the thermosphere, since the O's number density will be depleted and the N₂ is relatively stable. So the O/N₂ ratio is usually used as the indicator of the disturbance in the thermosphere. In addition, the Changes in O/N₂ have also been linked to changes in F-region peak electron density and total electron content as would be expected from photochemical equilibrium (Strickland et al., 2001; Immel et al., 2001; Lean et al., 2011). Consequently, establishing a method to retrieve the O/N₂ data, especially in a global scale, will be meaningful to monitor the disturbance in the thermosphere.

Observations and studies over the past half century have confirmed that magnetic storms and substorms can cause changes of the density of the neutral components (O, N₂, O₂) in the earth's thermosphere. Analysis of FUV data from the Global Ultraviolet Imager (GUVI) instrument on the NASA Thermosphere Ionosphere Mesosphere Energetics and Dyhof O/N₂ to dynamical processes in the thermosphere that can change the abundance of O relative to N₂ (Zhang et al., 2004; Meier et al., 2005, 2015; Crowley and Meier, 2013). Changes in the amount of O/N₂ are reflective of ascending and descending motions in the thermosphere. Ascending motion arises from energy input into the lower thermosphere and upper mesosphere from high-latitude forcing and tides. High-latitude forcing (Joule heating and energy deposition by particle precipitation) can produce strong upward movement in the heated regions, which in turn leads to strong decreases in O/N₂. Descending motion outside the heated regions leads to increases in the amount of O/N₂. The effects of high-latitude forcing and tides on thermospheric composition have been addressed in numerous papers reporting results from thermospheric general circulation models.

The FUV dayglow radiation, generated by the collision between photoelectrons and the neutral particles in the upper atmosphere,

* Corresponding author.

E-mail address: chen_bo_2019@163.com (B. Chen).<https://doi.org/10.1016/j.jastp.2020.105196>

Received 18 September 2019; Received in revised form 5 January 2020; Accepted 8 January 2020

Available online 3 February 2020

1364-6826/© 2020 Elsevier Ltd. All rights reserved.

includes the optical radiation signals of the main components (N_2 , O, O_2) in the ionosphere. Observations from space can obtain the densities and spatial distributions of the neutral components, thus providing a powerful way for monitoring the state of the upper atmosphere. At present, many remote sensing instruments have been used to observe the FUV radiations in space. Such as, the DE1/SAI (FUV in 120–170 nm), the Polar Bear/AIRS (OI 135.6 nm, LBH in 155–170 nm), the IMAGE/WIC (LBH in 140–180 nm), DMSP/SSUSI and TIMED/GUVI (H 1221.6 nm, OI 130.4 nm, OI 135.6 nm, LBH in 140–150 nm and 165–180 nm), FY-3D/WAI (FUV in 140–180 nm). Among them, OI 135.6 nm and N_2 LBH emissions are the two most important observations cause that the OI 135.6 nm radiation is considered to be the best signal for remote sensing detection of oxygen atom, and the N_2 LBH radiation is the strongest molecular radiation in all FUV emissions. Using the two FUV radiations can obtain the O/N_2 ratio.

Craven proposed that the FUV airglow data could be used to study the change of neutral components in the thermosphere in 1994 (Craven et al., 1994). Strickland did a theoretical study on the relation between FUV OI 135.6 nm and a more quantitative term, O/N_2 , defined as the column density ratio of O to N_2 referenced to a fixed column density of N_2 (Strickland et al., 1995). They demonstrated that the O/N_2 ratio is directly proportional to the intensity ratio of OI 135.6 nm to N_2 LBH viewed downward from satellite altitudes. And they used the spectral data (OI 135.6 nm and N_2 LBH in 140–170 nm) from DE1/SAI and the atmospheric model to obtain the O/N_2 ratio by construct a first-principles calculation of the intensity IIP with the solar zenith angle, the look angles and the ratios (Strickland and Cox, 1998). In 2004, Strickland used the AURIC algorithm to create a look table to find out the relationship between O/N_2 and OI135.6/LBHS and analyze the seasonal variation of O/N_2 in global thermosphere combining with the observations of TIMED/GUVI (Strickland et al., 2004). Zhang calculated the O/N_2 using the spectral intensities (OI 135.6 nm and N_2 LBHS) from TIMED/GUVI by fitting the simulations from AURIC algorithm and atmospheric model results to the observations (Zhang et al., 2004). The inversion approach used for retrieval of O/N_2 has also been applied to data from the Special Sensor Ultraviolet Limb Imager sensors on the DMSP F16-F19 satellite series (Dymond et al., 2017). Wang retrieved the O/N_2 through quantizing the OI135.6/LBH from TIMED/GUVI directly and used the ratio to track the process of magnetic storms (Wang et al., 2009). Peng used the AURIC algorithm to simulate the GUVI observations to retrieve the O/N_2 ratio and they normalized the look angles and SZA (Peng et al., 2012). Zhang studied the theoretical relationship between the OI 135.6 nm relative to N_2 LBH and the O/N_2 and they analyzed the solar effect on the retrieved ratios (Zhang et al., 2014). Andrew set up the daytime O/N_2 retrieval algorithm for the Ionospheric Connection Explorer (ICON) by updating the GUVI limb algorithm version (Stephan et al., 2018).

The algorithm in this paper was established by constructing the linear relationship between the O/N_2 ratio from model and the FUV dayglow components calculated by the Re-AURIC algorithm. This AURIC algorithm, developed by the Computational Physics, Inc (CPI) and the Air Force Phillips Laboratory/Geophysics Directorate, is often used to simulate and calculate the radiation transition in upper atmosphere (Strickland et al., 1999). The AURIC algorithm was modified through recalculating the geophysical parameters and updating the atmospheric and the ionospheric modules so that it can suit the application after 2000. The linear relationship was found out through the simulations of the observations on satellite by Re-AURIC, and these coefficients were used to derive the O/N_2 ratio from the SSUSI SDR data. The algorithm to calculate the global O/N_2 ratio, presented in this essay, will be used to convert the FUV measurements from Chinese FY-3D satellite into O/N_2 data products (Zhang et al., 2019).

In this paper we present an algorithm for interpreting simultaneously measured OI 135.6 nm and N_2 Lyman-Birge-Hopfield (LBH) disk dayglow emission from above the emitting region in terms of the abundance of atomic oxygen (O) in the thermosphere relative to N_2 . The

data sets are described in section 2, the method and the calculations are given in section 3. The obtained global O/N_2 ratio maps and its variations with magnetic storm will be analyzed in section 4, and the discussion and summary are in section 5.

2. Data sets

The Environmental Data Record (EDR) and Sensor Data Record (SDR) data used in this study were obtained by the DMSP F17 and F18 SSUSI instrument (Paxton et al., 2004; Sotirelis et al., 2013). The DMSP satellites were launched into circular polar orbits with orbital height of 840 km. From F16 through F18, the DMSP satellites were equipped with SSUSI, and the SSUSI data were available from 2004 on. It was designed to provide quantitative observations and interpretations of the Earth's airglow and auroral emissions in FUV. The optical systems is an imaging spectrograph with instantaneous FOV of 11.8° , and the observed wavelength is in five channels between 115 nm and 180 nm, in which, the OI 135.6 nm (band range: 134.2–137.7 nm) and the N_2 LBHS (band range: 140.0–150 nm) are used in this study.

The EDR data, available at <http://ssusi.jhuapl.edu/>, was used to determine the geophysical points to be calculated. The O/N_2 ratios, provided by the DMSP data process center, are also included in the EDR data and these can be as a reference to our calculations. After the accuracy and the feasibility were determined, the FUV dayglow components in the SDR data were used to derive the global O/N_2 ratio maps. The Dst indices, indicating the geomagnetic activity, are produced by NASA OMNIWeb Plus service. The viewing vector and the spectral range, driving the Re-AURIC, are set to be $108^\circ \sim 180^\circ$ and 120–180 nm respectively. Among that, 180° represents the nadir direction, the step of the viewing vector is 0.8° which can be used to simulate the SSUSI observations, and the spectral resolution is 0.1 nm.

3. Method and calculations

3.1. Re-AURIC

The AURIC v1.2 version released by CPI is only suit for the calculation before 2000 since the databases of F10.7 and Ap are from 1947 through 1999 and the modules of GEOPARM, ATMOS, and IONOS are all old. Therefore, in Re-AURIC, the databases are updated and the geophysical parameters (geomagnetic coordinates, magnetic dip angle, solar zenith angle, solar local time) are all recalculated. The dayglow execution flow diagram is shown in Fig. 1, in which, the GEOPARM module is recalculated and the ATMOS and the IONOS modules are replaced by the new models writing by the FORTRAN language. The magnetic dip angle is calculated by the International Geomagnetic

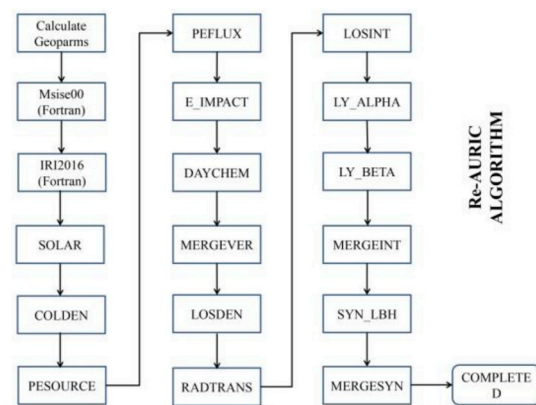


Fig. 1. The dayglow execution flow chart. The initial calculations in GEOPARM module are recalculated, and the atmospheric model and the ionospheric modules are replaced by Mssise00 and IRI2016.

Reference Filed (IGRF) (Finlay et al., 2010), the solar zenith angle is calculated based on the algorithm proposed by Reda (Reda and Andreas, 2004), and the new F10.7 and Ap are all derived from the database available at ftp://ftp.ngdc.noaa.gov/STP/GEOMAGNETIC_DATA/INDICES/KP_AP. The ATMOS module is replaced by the Msise00 atm model to calculate the atmospheric temperature and the densities of neutral atmosphere (N₂, O₂, O, O₃, NO, N, He, H, Ar). The IONOS module is replaced by the International Reference Ionosphere-2016 (IRI-2016). The electronic density, electronic temperature, ionic composition and ionic temperature in the altitude between 50 Km and 1500 Km can be all calculated using this model (Bilitza and Reinisch, 2008; Bilitza et al., 2014). After finishing the recalculations and replacements, the Re-AURIC can be applied to the present calculation and the initial inputs are only three parameters including geographic latitude, geographic longitude and the universal time (UT).

3.2. Method

A systematic study of FUV dayglow lines and bands of O and N₂ was carried out by Meier and Anderson (1983). Strickland put up that O (5S) and N₂ (α1Π) column density can be expressed as (in units of Rayleigh) (Strickland et al., 1995):

$$4\pi I_{OI1356}(\mu) = 10^{-6} \int_{z_l}^{z_u} j_{OI1356}(z) T(z, \mu) e^{-t(z)/\mu} dz / \mu \quad (1)$$

$$4\pi I_{LBHS}(\lambda, \mu) = 10^{-6} \int_{z_l}^{z_u} j_{LBHS}(z) f_\lambda e^{-t_\lambda(z)/\mu} dz / \mu \quad (2)$$

where z_l and z_u are referred to the lower and upper boundary of the calculated emission region, μ is cosine of the viewing angle, λ is the wavelength of the spectrum, f_λ is the fraction of j_{LBHS} at λ , $j_{OI135.6}$ is the volume emission rate including the effects of multiple scattering and j_{LBHS} is the total volume emission rate of LBHS, $t_\lambda(z)$ is the optical depth for pure absorption by O₂ at λ , and $T(z)$ is the transmission function for self-absorption by O. With reference to the research by Strickland (Strickland et al., 1995), the theoretical formula of O/N₂ can be represented as:

$$\frac{I_{OI1356}}{I_{LBHS}} \approx k \frac{\int_{N_T}^0 f_o(N_T) dN_T}{\int_{N_T}^0 f_{N_2}(N_T) dN_T} = k \frac{O}{N_2} \quad (3)$$

Where N_T is the total vertical column density. The formula shows that the OI135.6/LBHS is linearly related to O/N₂ so that the O/N₂ ratio can be determined after the linear coefficients are found out.

The observing angles need to be normalized to the nadir direction cause the SSUSI working mode. The Re-AURIC was used to simulate the SSUSI observations. The altitude was set to be 840 km which nearly equal to the height of DMSP satellite. The observing angles are set to be 108°~180° (180° is the nadir direction) with an interval of 0.8° referenced the SSUSI scanning pattern. The intensities of OI 135.6 nm and N₂ LBHS are then calculated under different observing angles. The normalized values between the nadir direction and the other directions are given in Fig. 2.

Similarly, the solar zenith angles (SA) are also need to be normalized along different lines of sight (LOS). During the calculations, the SZA range between 0° and 90° with an interval of 10° was chosen to calculate the intensities of OI 135.6 nm and N₂ LBHS. The normalized values to 0° of SZA are shown in Fig. 3.

3.3. O/N₂ ratios

After the normalized values of observing angles and SZA are calculated, the relationship between OI135.6/LBHS and O/N₂ ratio can be determined using the data files from Re-AURIC. Fig. 4 shows the correlations of the simulated OI135.6/LBHS and O/N₂ ratio. As we can see,

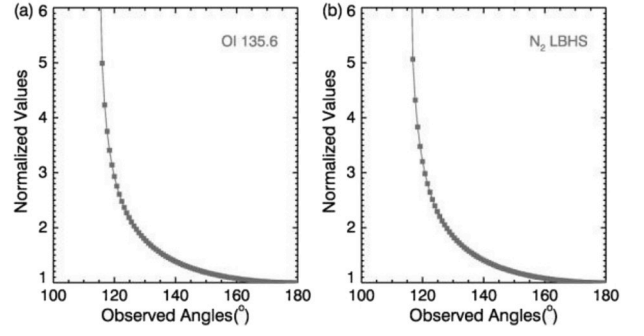


Fig. 2. The normalized values of observing angles for OI 135.6 nm and N₂ LBHS data from Re-AURIC.

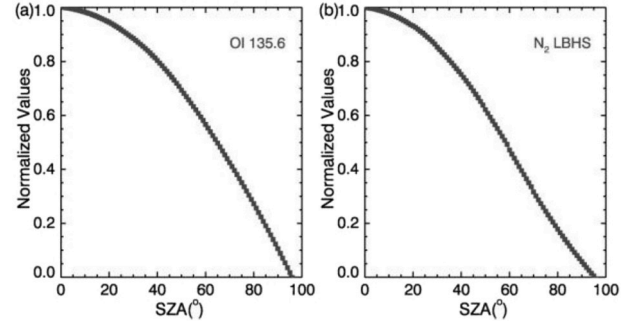


Fig. 3. The normalized values of SZA for OI 135.6 nm and N₂ LBHS data from Re-AURIC.

the relationship can be well interpreted by a linear fitting with a high correlation coefficient (CC = 0.989). The red solid line in Fig. 4 is a minimum square fitting line that can be represented by an equation

$$O / N_2 = 0.934 \times OI356/LBHS - 0.202 \quad (4)$$

To verify the validity of the linear coefficients, the O/N₂ data from SSUSI EDR data set was extracted to compare with the calculations. The two data sets are corresponded one by one at the same time and in the same geophysical location. Finally, 1137 pairs of points are identified and the scatter plots of these pairs are shown in Fig. 5. All the scatters are linearly fitted to straight line of O/N₂-Cal = A + B × O/N₂-EDR as shown in the figure. The uncertainties of A and B are 0.012 and 0.024. The black solid line in Fig. 5 indicates O/N₂-Cal = O/N₂-EDR, that is O/N₂-Cal and O/N₂-EDR agree perfectly, and the dashed lines are plotted at O/N₂-Cal = O/N₂-EDR ± 0.2. The standard deviation (1σ) and the

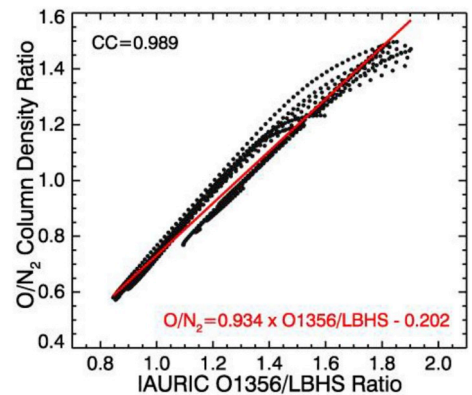


Fig. 4. The simulated linear relationship of O/N₂ and OI 135.6/LBHS from Re-AURIC. The red line is the linear fitting and the linear formula is at the right lower corner. The correlation coefficient is at the left upper corner.

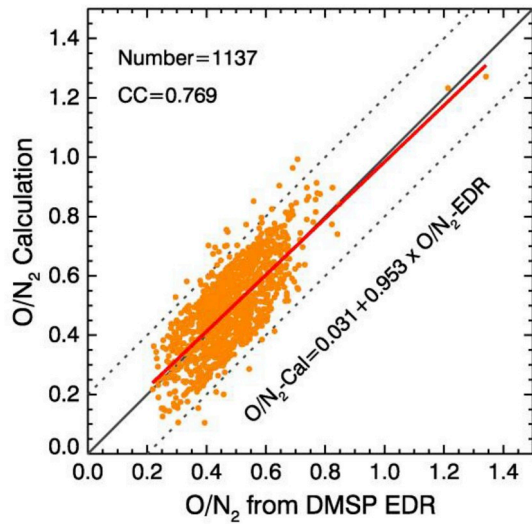


Fig. 5. Comparisons between calculated O/N_2 and the ratios from DMSP SSUSI EDR data sets. The black solid line indicates $O/N_2\text{-Cal} = O/N_2\text{-EDR}$, and the dash lines are plotted at $O/N_2\text{-Cal} = O/N_2\text{-EDR} \pm 0.2$, respectively. The red solid line is the linear fitting of $O/N_2\text{-EDR}$ to $O/N_2\text{-Cal}$ with the correlation coefficient shown in the upper left corner. The number of samples is 1137.

correlation coefficient between the calculated O/N_2 ratios and the EDR values are 0.045 and 0.769, respectively. The statistical errors between the calculated ratios and the EDR references are generally less than 0.2 with 96.40% at 2σ (95.44%) and less than 0.1 with 60.51% at about 1σ (68.26%). Fig. 5 demonstrates that our algorithm used to calculate the O/N_2 ratio is correct and reliable given that the EDR values are reliable.

4. Global variations

Two global O/N_2 ratio maps are derived using this algorithm to study the variations of the ratios during geomagnetic storm. The OI 135.6 nm and N_2 LBHS data are from SSUSI SDR data and the dates are January 11, 2018 and May 5, 2018 respectively. The Dst indices in the two days are plotted in Fig. 6. Fig. 6 shows that the geomagnetic activities are quiet in 11 January and disturbed in 5 May.

The global O/N_2 ratio maps are shown in Fig. 7 and Fig. 8. Fig. 9 shows the variation of O/N_2 along longitude 116° E where Beijing located. This longitude was chosen arbitrarily to reveal the variations. The O/N_2 depletion appears in Fig. 8 with the development of the magnetic storm comparing with Fig. 7. Note that the expansion of the

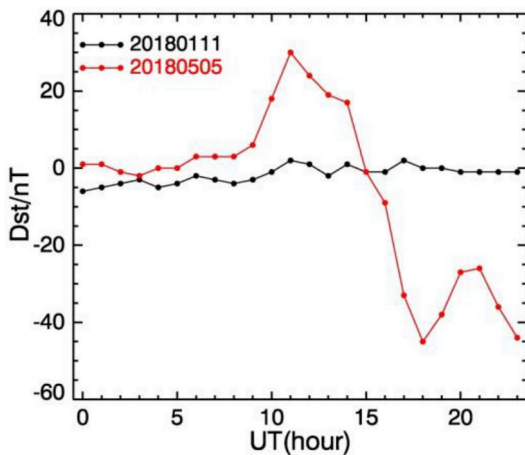


Fig. 6. The Dst indices in January 11, 2018 and May 5, 2018. Magnetic storm occurred in May 5, 2018.

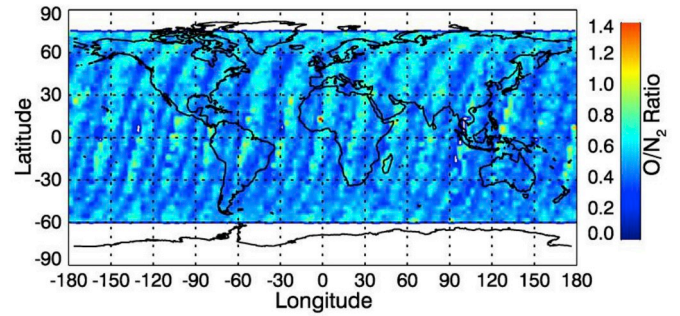


Fig. 7. The global O/N_2 ratio map on January 11, 2018 from SSUSI 14 orbits. The abscissa is longitude and the ordinate is latitude.

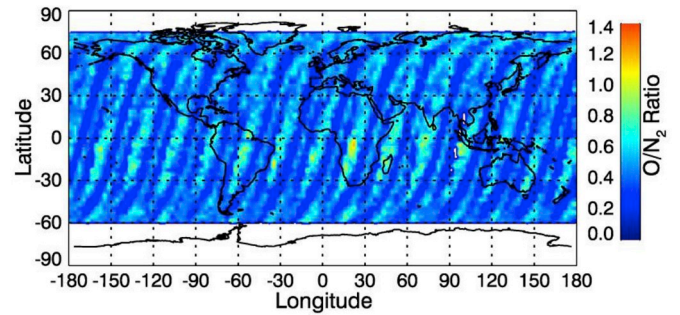


Fig. 8. Similar to Fig. 7, but for May 5, 2018.

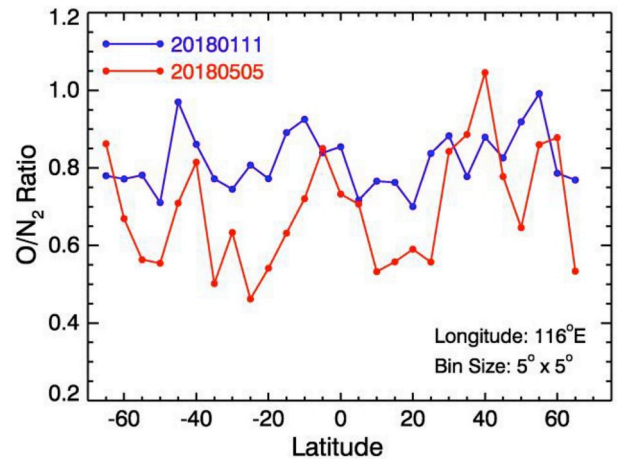


Fig. 9. Variation of the O/N_2 ratios along longitude 116° E. The values are from Fig. 7 (blue line) and Fig. 8 (red line) and binned with 5° (longitude) \times 5° (latitude).

depletion is not uniform at different longitudes. Meanwhile, the depletion scales, extending from high latitude to low latitude, can be seen in the two O/N_2 maps. Many studies have shown that intense Joule and particle heating causes strong upwelling of the atmosphere around the auroral oval during a geomagnetic storm, and the strong atmospheric upwelling transports the decreased O or the increased N_2 air up from much lower in the thermosphere into the F -region (Mayr and Volland, 1972; Mayr et al., 1978; Pröls, 1980). Then, the neutral winds can redistribute this particular air over much of the high-latitude region and part of the middle-latitude region. The disturbed region can extend to middle or even low latitude with a sufficiently strong wind surge. Also, some researches show that the composition changes are due to an overall depletion of O throughout the lower thermosphere extending up to F -region heights with enhancements in N_2 at higher altitudes (Mayr

and Volland, 1972; Pröls et al., 1988; Burns et al., 1989).

5. Discussion and summary

An algorithm to derive the global O/N₂ ratio was proposed in this investigation. The algorithm was developed by determined the linear coefficients between the simulated OI 135.6 nm and N₂ LBHS intensities from Re-AURIC and the O/N₂ ratio from atmospheric model. Comparison between the derived data and the O/N₂ ratio from SSUSI EDR was analyzed and high consistency demonstrated that the algorithm is effective and feasible. Also, two global O/N₂ ratio maps during magnetic quietness and storm, calculated by the algorithm, were investigated. The studies show that the O/N₂ ratios appear a significant depletion with the development of the magnetic storm in a global scale, and the expansion of the depletion, extending from high latitude to low latitude, is not uniform at different longitudes. The calculation method of O/N₂ is summarized as follow:

- (1) Updating the AURIC algorithm to Re-AURIC.
- (2) Simulating the observation pattern of SSUSI and calculating the OI 135.6 nm and N₂ LBHS intensities.
- (3) Normalizing the observation angles to nadir direction.
- (4) Normalizing the SZA along the LOS to 0°.
- (5) Extracting the O and N₂ components from the Msise00 model.
- (6) Determining the correlation coefficients between the simulated intensities and O/N₂ ratio.
- (7) Deriving the global O/N₂ map using the coefficients and SSUSI SDR data.

This proposed method provides us with a useful tool to obtain the global O/N₂ distribution. Using this algorithm, we plan to derive the O/N₂ ratio combining the FUV data from Chinese FY-3D satellite (Zhang et al., 2019), and establish an empirical model of the O/N₂ depletion versus the solar wind, IMF parameters and the heating rate in the future. This will be useful for the nowcasting and forecasting of the space weather.

Acknowledgement

This work was supported by National Natural Science Foundation of China (Grant No. Y6983JA).

References

Bilitza, D., Reinisch, B.W., 2008. International reference ionosphere 2007: improvements and new parameters. *Adv. Space Res.* 42, 599–609.

Bilitza, D., Altadill, D., Zhang, Y., et al., 2014. The international reference ionosphere 2012—a model of international collaboration. *J. Space Weather Space Clim.* 4, 1–12.

Burns, A.G., Killen, T.L., Roble, R.G., 1989. Causes of changes in the composition calculated using a thermospheric general circulation model. *J. Geophys. Res.* 94, 3670.

Craven, J.D., Nicholas, A.C., Frank, L.A., et al., 1994. Variations in FUV dayglow brightness following intense auroral activity. *Geophys. Res. Lett.* 21, 2793.

Crowley, G., Meier, R.R., 2013. Disturbed O/N₂ Ratios and Their Transport to Middle and Low Latitudes. *Am. Geophys. Union, Washington.*

Dymond, K.F., Nicholas, A.C., Budzien, S.A., et al., 2017. The special sensor ultraviolet limb imager instruments. *J. Geophys. Res.* 122, 2674–2685.

Evans, J.S., Strickland, D.J., Huffman, R.E., 1995. Satellite remote sensing of the thermospheric O/N₂ and solar EUV, 2, Data analysis. *J. Geophys. Res.* 100, 12227.

Finlay, C.C., Maus, S., Beggan, C.D., et al., 2010. International geomagnetic reference field: the eleventh generation. *Geophys. J. Int.* 183, 1216–1230.

Immel, T.J., Crowley, G., Craven, J.D., et al., 2001. Dayside enhancements of thermospheric O/N₂ following magnetic storm onset. *J. Geophys. Res.* 106, 15471–15488.

Lean, J.L., Meier, R.R., Picone, J.M., et al., 2011. Ionospheric total electron content: global and hemispheric climatology. *J. Geophys. Res.* 116, A10318.

Mayr, H.G., Volland, H., 1972. Magnetic storm effects in the neutral composition. *Planet. Space Sci.* 20, 379.

Mayr, H.G., Harris, I., Spencer, N.W., 1978. Some properties of upper atmosphere dynamics. *Rev. Geophys.* 16, 539.

Meier, R.R., Anderson, D.E., 1983. Determination of atmospheric composition and temperature from the UV dayglow. *Planet. Space Sci.* 31, 967.

Meier, R., Crowley, G., Strickland, et al., 2005. First look at the 20 November 2003 superstorm with TIMED/GUVI: comparisons with a thermospheric global circulation model. *J. Geophys. Res.* 110, A09S41.

Meier, R.R., Picone, J.M., Drob, D., et al., 2015. Remote sensing of Earth's limb by TIMED/GUVI: retrieval of thermospheric composition and temperature. *Earth Space Sci.* 2, 1–37.

Paxton, L.J., Christensen, A.B., Morrison, D., et al., 2004. GUVI: a hyperspectral imager for geospace. *Proc. SPIE* 5660, 228–240.

Peng, S.F., Tang, Y., Wang, J., et al., 2012. Research on retrieving thermospheric O/N₂ from FUV remote sensing. *Spectrosc. Spectr. Anal.* 32, 1296–1300.

Pröls, G.W., 1980. Magnetic storm associated perturbations of the upper atmosphere: recent results obtained by satellite-borne gas analyzers. *Rev. Geophys.* 18, 183.

Pröls, G.W., Moemer, M., Slowey, J.W., 1988. Dissipation of solar wind energy in the Earth's upper thermosphere: the geomagnetic activity effect. *Adv. Space Res.* 8 (5–6), 215.

Reda, I., Andreas, A., 2004. Solar position algorithm for solar radiation application. *Sol. Energy* 76, 577–589.

Sotirelis, T., Korh, H., Hsieh, S.Y., et al., 2013. Empirical relationship between electron precipitation and far ultraviolet auroral emissions from DMSO observations. *J. Geophys. Res.* 118, 1203–1209.

Stephan, A.W., Meier, R.R., England, S.L., et al., 2018. Daytime O/N₂ retrieval algorithm for the ionospheric connection explorer (ICON). *Space Sci. Rev.* 214, 42.

Strickland, D.J., Cox, R.J., 1998. Global O/N₂ derived from DE 1 FUV dayglow data: technique and examples from two storm periods. *J. Geophys. Res.* 104 (A3), 4251–4266.

Strickland, D.J., Evans, J.S., Paxton, L.J., 1995. Satellite remote sensing of thermospheric O/N₂ and solar EUV, 1, Theory. *J. Geophys. Res.* 100, 12217.

Strickland, D.J., Bishop, J., Evans, J.S., et al., 1999. Atmospheric ultraviolet radiance integrated code (AURIC): theory, software architecture, inputs, and select results. *J. Quant. Spectrosc. Radiat. Transfer* 62, 689–742.

Strickland, D.J., Craven, J.D., Daniell, R.E., 2001. Six days of thermospheric-ionospheric weather over the Northern Hemisphere in later September 1981. *J. Geophys. Res.* 106, 30291–30306.

Strickland, D.J., Meier, R.R., Walterscheid, R.L., et al., 2004. Quiet time seasonal behavior of the thermosphere seen in the far ultraviolet dayglow. *J. Geophys. Res.* 109, A01302.

Wang, J., Tang, Y., Tang, L.J., et al., 2009. Retrieval of Ionospheric O/N₂ based on FUV imaging data. *SPIE Proc.* 7498, 74982N.

Zhang, Y., Paxton, L.J., Morrison, D., et al., 2004. O/N₂ changes during 1–4 October 2002 storms: IMAGE SI-13 and TIMED/GUVI observations. *J. Geophys. Res.* 109, A10308.

Zhang, Y.C., Zhang, X.X., He, F., et al., 2014. Retrieving O/N₂ technique from ionospheric FUV dayglow emissions. *Optic Precis. Eng.* 22, 1120–1128.

Zhang, X.X., Chen, B., He, F., et al., 2019. Wide-field auroral imager onboard the Fengyun satellite. *Light Sci. Appl.* 8, 47.